Astron. Astrophys. 362, 255–262 (2000)

ASTRONOMY AND ASTROPHYSICS

Strong asymmetries in the neutral envelope of Mira⋆

CO and K I observations

E. Josselin[1,2], **N. Mauron**[2], **P. Planesas**[1], **and R. Bachiller**[1]

[1] Observatorio Astronómico Nacional (OAN), IGN, Apartado 1143, 28800 Alcalá de Henares, Spain
[2] Groupe d'Astrophysique, CC72, CNRS/U. Montpellier II, Place E. Bataillon, 34095 Montpellier Cedex, France

Received 12 April 2000 / Accepted 4 July 2000

Abstract. We present high-resolution observations of the neutral envelope of o Ceti. The molecular component has been mapped in the CO(2–1) radio line and the atomic component is studied through long-slit spectroscopy of the optical KI line. These observations reveal strong asymmetries in the gas distribution, which can be interpreted as a spherical envelope disrupted by a bipolar outflow.

These data, combined with other observations of this object as well as similar observations of other AGB stars, suggest that asymmetrical mass loss processes occur early during the AGB stage, well before the proto-planetary nebula phase.

Key words: stars: AGB and post-AGB – stars: circumstellar matter – stars: individual: o Ceti

1. Introduction

After leaving the main sequence, low- and intermediate-mass stars ($M_{init} \lesssim 8\,M_\odot$) evolve towards the planetary nebula (PN) stage, through the red giant branch and the asymptotic giant branch (AGB). The AGB phase is characterized by strong mass loss, at a rate $\dot{M} \gtrsim 10^{-7}\ M_\odot\ yr^{-1}$, which generates circumstellar envelopes (CsE) made of atomic and molecular gas, and dust. These components are observed over a large wavelength range, from the optical domain up to the radio domain. The interpretation of these observations generally assumes spherical symmetry and a steady mass loss (e.g. Knapp & Morris 1985, Jura 1986, Mauron & Caux 1992, Olofsson et al. 1993). This allows the determination of mass-loss rates, with probably a reasonable accuracy, i.e. within a factor of about two, and of physical quantities such as abundances (Olofsson 1999).

However, the recent progresses in observational techniques and the improved spatial resolution have put in evidence that many CsE display departures from spherical symmetry (e.g. Knapp et al. 1998, Lopez 1999). In particular, asymmetries seem to be common among objects presumably on the AGB tip. Moreover, many PNe are known to be elliptical or bipolar. Outstanding questions are therefore how and when such asymmetry appears during the AGB evolution.

Mira (o Ceti), the prototype of long period variable stars, is particularly well-suited to tackle with these problems, since it is one of the closest oxygen-rich AGB stars. This object is in fact a binary, maybe even a triple system (see Karovska et al. 1993). The atmosphere of the AGB star of this system (Mira A) appears elliptical (Haniff et al. 1992, Karovska et al. 1997). Its companion (Mira B) is still of uncertain nature, being a main-sequence star or a white dwarf. It is relatively hot (about 10000 K), maybe also asymmetric and maybe surrounded by an accretion disk (Karovska et al. 1997). The main characteristics of this system are summarized in Table 1.

Table 1. General properties of o Ceti.

Coordinates		Ref.
α (J2000.0)	02:19:20.72	1
δ (J2000.0)	–02:58:39.4	1
$15\mu_\alpha\cos\delta$	–0.009″/yr	1
μ_δ	–0.237″/yr	1
Distance	131 ± 18 (1σ) pc	2
Spectral type	M6e - M9e II	3
Pulsation period	331 days	3
m_V	2.0 (max) to 10.1 (min)	3
L_{mean}	6500 $L_\odot$	4
T_{eff}	2350 K	4
Stellar asymmetry		
Axial ratio	0.82	5
P.A.	120°	5
Companion (Mira B)		
Separation	0.58″	5
P.A.	108°	5
Period of revolution	$\gtrsim$ 400 yrs	5

1: HIPPARCOS Input Catalogue (HIC).
2: HIPPARCOS Catalogue (HIP).
3: General Catalogue of Variable Stars.
4: Barthes & Mattei (1997).
5: Karovska et al. (1997).

Send offprint requests to: E. Josselin (josselin@oan.es)

⋆ Based on observations carried out with the IRAM Plateau de Bure Interferometer, the Canada-France-Hawaii Telescope, and at the Haute-Provence Observatory. IRAM is supported by INSU/CNRS (France), MPG (Germany) and IGN (Spain).

The CsE of o Ceti has a rather rich molecular content, with ^{12}CO, ^{13}CO, ^{28}SiO, ^{29}SiO, H_2O, OH, HCN, and (tentatively) CN lines detected (see e.g. Wooten et al. 1982, Bujarrabal et al. 1994, Herpin et al. 1998). Neither SO or SO_2 have been detected, as it could be expected in such an oxygen-rich medium. This may indicate the weakness of shocks in the envelope (Sahai & Wannier 1992, Omont et al. 1993).

The first detailed study of the geometry of the molecular CsE of o Ceti has been carried out by Planesas et al. (1990a and 1990b). They showed that the CO spectra contain three velocity components, corresponding to a dominant spherical envelope with an expansion velocity of 7 km s^{-1} and a poorly collimated, low velocity ($V_{exp} \sim 4$ km s^{-1}) bipolar outflow. This seems confirmed by their maps at 6″ resolution, which display two lobes of an axial gas outflow, oriented roughly North-South. The atomic component of the envelope also displays indications of asymmetry, as shown by Mauron & Caux (1992) from observations of stellar light scattered by circumstellar atomic gas in the KI and NaI lines. The KI peculiar profiles suggested a non-spherical, optically thin envelope.

This paper reports new high angular resolution observations of the neutral envelope of o Ceti, in the millimeter CO(2–1) line and the optical KI lines. The observations and data reduction are described in Sect. 2. Our results are given in Sect. 3 and discussed in the context of circumstellar asymmetries in Sect. 4.

2. Observations and data reduction

2.1. Millimeter observations

2.1.1. CO and SiO mapping

Interferometric observations, centered on o Ceti, were made with the IRAM interferometer (Plateau de Bure, near Grenoble, France; Guilloteau et al. 1992) from December 1995 to March 1996. We observed two lines, CO(2–1) and SiO(v=0,J=2–1), with three configurations of the array, C1, C2 and D. At that time the array consisted of four 15m antennas. At the frequency of the CO(2–1) line, the primary beam of each antenna was 22″ (FWHM). During each of the observing periods, the meteorological conditions were good with precipitable water vapor rather constant, around 2.5 mm and a seeing better than 1.5″.

Four quasars, 0923+392 (flux density = 2.20 Jy at 230 GHz), 3C454.3 (3.04 Jy), 0415+379 (7.00 Jy) and 0420-014 (2.70 Jy), were also observed to ensure the radio-frequency passband and amplitude calibration. Later observations showed that the coordinates of the phase calibrator J0241-0815 (0.50 Jy) used during these observations, were wrong ($\Delta\alpha \sim 7''$ and $\Delta\delta \sim 3''$), leading to a slight deterioration of pointing (presumably of the order of 1″) and phase accuracy.

Data reduction was performed with the GILDAS software, developed at IRAM and Grenoble Observatory. It included calibration of passband, phase and amplitude, map restoring and CLEANing with the CLARK method.

Concerning CO data, we used as zero-spacing observations the single-dish data obtained at the IRAM 30m telescope 8 years before by Planesas et al. (1990a). This was done because the rather extended emission region induced the loss of large scale emission, inherent to the interferometric technique. This loss can reach 50% for envelopes larger than 20″ (Neri et al. 1998). Regarding the large proper motion of o Ceti and the difference between the epochs of single-dish and interferometric observations, we had to force the coordinates of the center of the 30m observations to be identical to those used at the Plateau de Bure. This unfortunately induces a loss of accuracy in absolute astrometry, but we verified that a small shift ($\sim 2''$) of the positions of the 30m observations does not affect the resulting combined map. The restored gaussian clean beam for the CO(2–1) observations is $2.5'' \times 2.4''$ at a position angle of 6°. For the SiO(v=0,J=2–1) observations, it is $4.7'' \times 3.6''$ at a position angle of 6°.

The thermal SiO(v=0,J=2–1) emission is not resolved in the North-South direction and extends less than 2″ in the East-West direction. The total SiO flux is 9.2 ± 0.1 Jy km s^{-1}. The emission peaks at the same velocity as the CO one. Besides the new upper limit for the size of the emitting region, our SiO data do not provide new significant pieces of information with respect to previous ones (Planesas et al. 1990a), so they will not be discussed hereafter.

2.1.2. Continuum emission

The IRAM continuum correlator was mainly used for calibration purposes. However, as a by-product of these observations, we measured the continuum emission at 1.3 mm. It is unresolved and has a flux of 50 mJy. This is lower by about a factor two than the flux measured by Walmsley et al. (1991), who found 116 mJy. We note that our measurement is in good agreement with the expected purely photospheric millimeter continuum (57 mJy) as found from extrapolation from 2.2 μm data given by Walmsley et al. (1991) and for the stellar temperature quoted in Table 1.

2.2. Optical observations of the KI lines

Long-slit spectroscopy of the envelope of o Ceti in the KI 7664.911 and 7698.974 Å lines was done at the Canada-France-Hawaii Telescope and the Haute-Provence Observatory. The main technical characteristics of these observations are given in Table 2. Our goal was to detect the faint outer parts of the envelope. Consequently the slit was placed at perpendicular distances between 5″ and 20″ from the star. The spectral resolution was chosen to be ∼1 Å. This is of the order of the width of the KI lines which consequently remain unresolved. Calibration exposures with the slit centered on the star were also achieved, including a few with widened slit for measuring the stellar flux through a neutral filter with density ∼2.

For each pixel along the slit located off-star, one obtains a linear spectrum consisting of sky emission lines, shell emission lines and the contaminating stellar scattered light. This last component can be removed by scaling and subtracting the on-star spectrum (see Mauron & Caux 1992, Plez & Lambert 1994). The result is a net spectrum which shows the shell KI lines and

sky lines. We measured the fluxes for both KI lines through integration over wavelength for every position along the slit.

The KI 7665 Å line can be affected by the nearby 7664.872 Å and 7665.944 Å O_2 telluric absorption lines (Chaffee & White 1982). This depends on the apparent radial velocity V_{app} of the source with respect to the observer. During the OHP observations, V_{app} was 84.3 km s^{-1}, yielding to a shift of 2.15 Å. This is sufficient to avoid any mutilation of the 7665 Å line. On the contrary, during the CFHT observations, V_{app} was only 28.9 km s^{-1}. Consequently, the circumstellar KI 7665 line, if centered at the mean circumstellar velocity (V_{LSR}= 46.5 km s^{-1}), lies between the two O_2 lines mentioned above. Any additional shift, e.g. due to motions of in the envelope, will provoke strong mutilation. On the contrary, no such absorption affects the 7699 Å line.

Concerning the surface brightness of the envelope in the KI 7699 line, the calibrations mentioned above and done on the star itself allow to derive, for every point along the slits, a surface brightness B, in units of Å arcsec^{-2}, normalized to the stellar flux near λ = 7699 Å. We then consider the product $H = B\,\theta^3$, θ being the distance to the star, which would be constant in the case of a wind with density varying in r^{-2} and optically thin line scattering (see details in Guilain & Mauron 1996). OHP measurements of the line flux peaks on each slit give values of H ranging from 3300 to 5000 10^{-6} Å arcsec, in good agreement (given the observational uncertainties) with the range 3800–10400 10^{-6} Å arcsec obtained by Mauron & Caux (1992). However, the values of H derived from CFHT observations of the peaks on each slit lie in the range 700–1000 10^{-6} Å arcsec, i.e. a factor of $\sim$ 5 smaller. In addition, surface brightness at the intersections of OHP and CFHT slits also indicates smaller brightness for CFH data, by a factor $\sim$ 2–4. We could not find any clear experimental explanation to this discrepancy. One possibility could be temporal variations of the KI density, due to changes in the KI ionization because of eventual long-term variations of the stellar UV flux. Anyhow, these uncertainties and calibration difficulties do not affect the following results, based on the relative spatial variations of the KI fluxes along each slit, which are much better known.

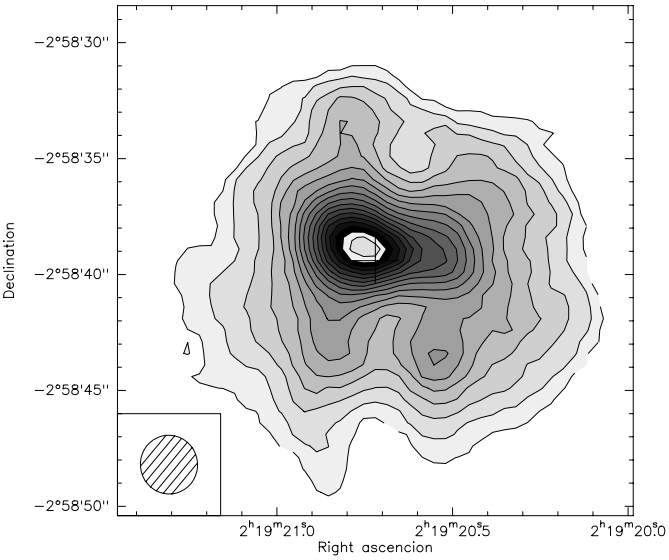

Fig. 1. Contour map of the integrated ^{12}CO(2–1) emission from *o* Ceti over the whole velocity range of emission. The lower level contour and the contour spacing are 2 Jy beam^{-1} km s^{-1}. The beam after cleaning is shown in the box in the lower left corner.

Table 2. Characteristics of optical observations.

Telescope	CFHT 3.6m	OHP 1.93m
Date	1992 July 5	1997 January 2 and 5
Spectrograph	Herzberg	Carelec
Long slit	130″ × 0.75″	333″ x 1.67″
Grating	830 lines mm^{-1}	1200 lines mm^{-1}
Detector	PHX CCD 512^2	TEK CCD 512^2
Dispersion	0.97 Å pix^{-1}	0.85 Å pix^{-1}
Scale on slit	0.61″ pix^{-1}	1.10″ pix^{-1}
Slit direction	north-south	east-west
Slit offset	5″W, 10″W	10″N, 19″N, 8″S
Exposure times	100s, 17mn	20mn, 10mn, 10mn

3. Results

3.1. The molecular gas

The overall distribution of the molecular gas as observed in the CO(2–1) line is shown in the velocity-integrated map in Fig. 1. The emission extends over 250″^{2}, which corresponds to a sphere of radius 1.7 10^{16} cm for a distance of 130 pc. Taking a stellar radius of $\sim$500 R$_\odot$, derived from the stellar parameters given by Barthes & Mattei (1997) based on a model with pulsations in the 1^{st} overtone, one finds that the CO envelope has an extension of $\sim$ 500 stellar radii. This extension is smaller by a factor of about 10 than the generic size usually assumed for statistical studies of AGB stars (Knapp & Morris 1985) but is fully consistent with the low mass-loss rate of *o* Ceti (10^{-7} M$_\odot$ yr^{-1}, Mauron & Caux 1992 and references therein). For such a value of the mass-loss rate, Mamon et al. (1988) showed that photodissociation by interstellar UV radiation is very efficient, with negligible self-shielding effects, and determines the extent of the molecular envelope. The observed size of the CO envelope is compatible with their model (see their Fig. 4).

We measured a total CO flux of 436 Jy km s^{-1}. This gives a CO column density of 7 10^{16} cm^{-2} for an excitation temperature of 70 K (Planesas et al. 1990a). Assuming a CO abundance with respect to H_2 of 5 10^{-4}, this corresponds to a mass of 1.5 10^{-4} M$_\odot$ for the molecular envelope. Combined with a mass-loss rate of 10^{-7} M$_\odot$ yr^{-1}, we obtain a dynamical age of 1500 years, assuming constant mass-loss rate. This is fairly consistent with the kinematic age (770 years) obtained by dividing the radius of the CO envelope by the expansion velocity, regarding the uncertainty on the relevant quantities and the fact that the CO extension is reduced because of photodissociation. Such low values are consistent with the idea that *o* Ceti still has not evolved far on the AGB stage, as suggested by its low mass-loss rate.

It is obvious that the circumstellar envelope significantly deviates from sphericity. The inner region is much more extended

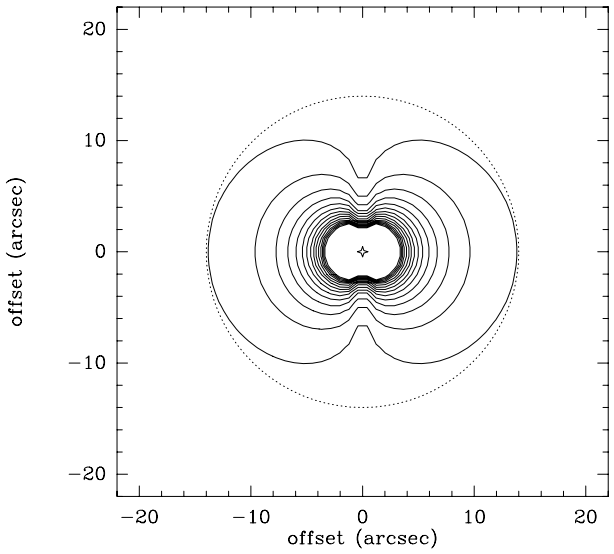

Fig. 2. Intensity map for a density distribution $n(r) \propto \cos^{1/2}(\theta)\, r^{-2}$, assuming optically thin emission and constant excitation conditions. A dashed circle has been drawn to emphasize the resulting departure from sphericity.

in the East-West direction than the North-South one. The most striking characteristic is the presence of two "holes" located at $\sim 4''$ North and South of the star position. These holes generate a butterfly-like structure. Such a morphology can be reproduced with a density law of the form $n(r) \propto \cos^{i}(\theta)\, r^{-2}$, with θ being the angle measured from the equatorial plane and $0 < i < 1$, as shown in Fig. 2. Interestingly, trigonometric laws of mass loss have already been invoked to explain the shaping of planetary nebulae in a two interacting wind model (Reimers et al. 1999).

The detailed structure and kinematics of the molecular gas can be seen in the channel maps in Fig. 3. The integrated blue and red fluxes are similar. Emission extends over a velocity range of ~ 7 km s^{-1}, the blue emission being visible over a wider range than the red one, by ~ 1 km s^{-1}. A bipolar structure appears, clearly when comparing channels symmetric in velocity. For instance, in the 44.5–44 and 48.5–49 km s^{-1} channels, the blue emission is distributed at the north of the star, whereas the red emission is distributed at the south. In most velocity channels, the blue emission is dominated by a kind of equatorial bar, which in Fig. 1 appears as an asymmetric "peanut". On the contrary, this bar is hardly visible in the red emission, which displays a butterfly-like shape, with brighter South-East wing.

Fig. 4 displays two velocity-position diagrams, built from cuts at central right ascension (top panel) and central declination (bottom panel). On the East-West cut, no particular feature appears. The emission is similar in each of the quadrants which delineate blue and red velocity and East and West parts of the envelopes. This diagram is characteristic of an expanding envelope which could be nearly spherical. On the contrary, on the North-South cut a clear asymmetry is observed, with blue emission excess in the North and red excess in the South. This corresponds to the three velocity components observed by Planesas et al. (1990a). The two holes are located at velocities $\sim$43 and

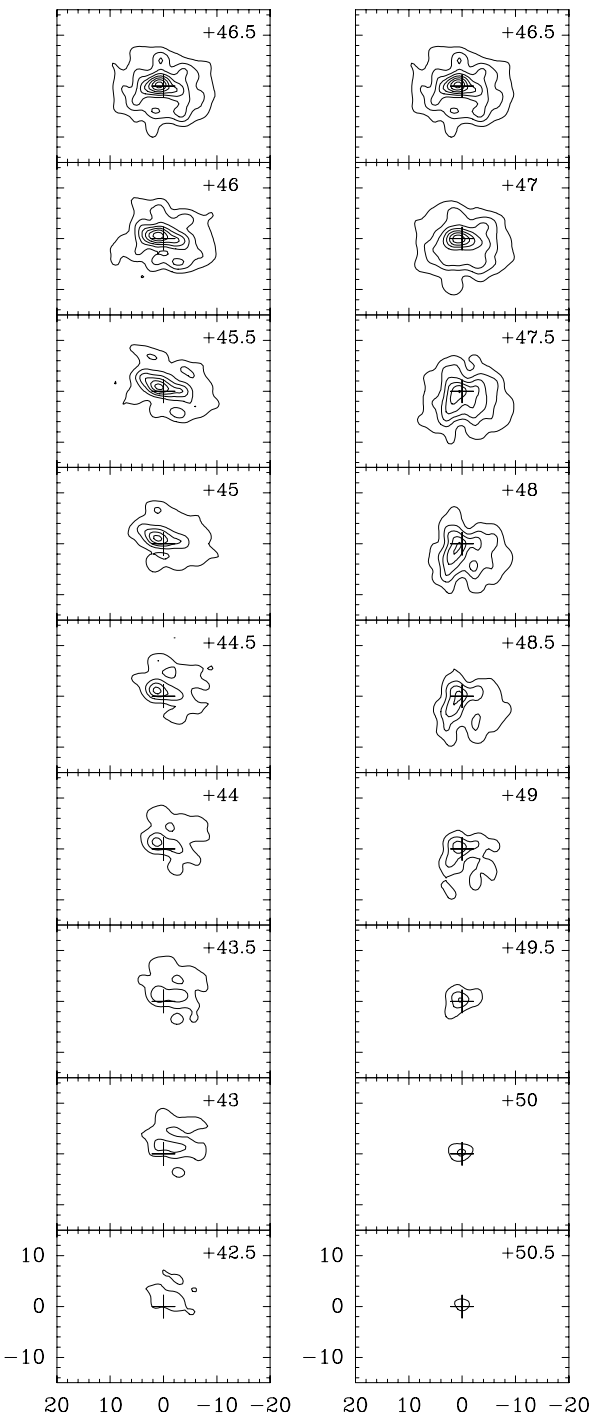

Fig. 3. Contour map of the ^{12}CO(2–1) emission integrated over equally spaced velocity channels with width of 0.5 km s^{-1}. The left column corresponds to the blue-shifted emission and the right column to the red-shifted emission. In each column the top panel displays the emission at the adopted stellar velocity (46.5 km s^{-1}). The lower level contour and the contour spacing are 1 Jy beam^{-1} km s^{-1}. The central LSR velocity for each panel is indicated in the top right corner.

$\sim$50 km s^{-1}. The tilt of the bipolar outflow is also seen, the holes being displaced from one to the other by about $10''$. This gives an inclination of about 30° and deprojected outflow veloc-

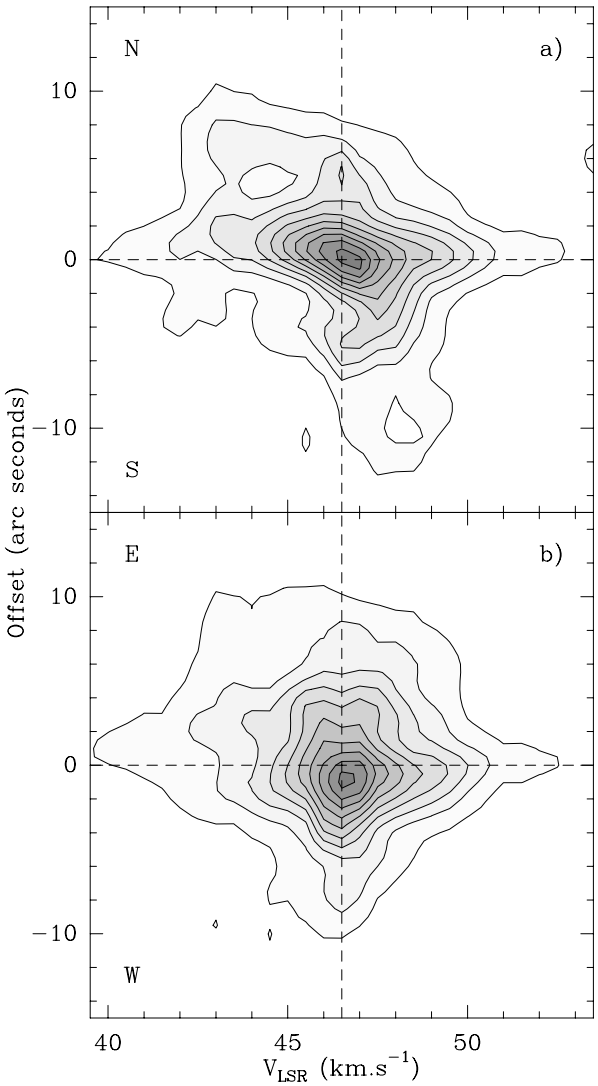

Fig. 4a and b. Velocity-position diagrams in the ^{12}CO(2–1) line obtained from cuts at declination offset = 0 (bottom panel) and R.A. offset = 0 (top panel).

ity of about 8 km s^{-1}. With such a low velocity, the outflow can certainly not generate strong shocks, which is consistent with the lack of SO and SO_2 emission evoked in the introduction.

Altogether, we thus see a rather spherical circumstellar envelope being disrupted by a low-velocity bipolar outflow.

3.2. The atomic gas

The brightness distribution of the $\lambda\lambda$ 7665, 7699 Å KI lines informs on the scattering of stellar light by circumstellar atomic potassium. The results of the observations along five slits (5 and 10″ W, 10 and 19″ N, and 8″ S) as well as the slit positions overimposed on the integrated CO emission map are shown in Fig. 5. The slit located at 5″ West, cuts the CO envelope at approximatively half its radius. The other slits are more distant from the star and probe regions where no CO is detected. The KI emission is seen up to a distance of 30″ from the star. This distance probably reflects the sensitivity limit and corresponds to $\sim$ 3.5 times the CO outer radius.

A striking characteristics of the KI spatial distributions along the slits is their asymmetries. These asymmetries can be explained by a structure in the north-west region, such as the bipolar outflow invoked to explain the radio map, superimposed on a spherically symmetric component. When the slit passes across this outflow in which the density is larger than in the surrounding spherical envelope, then an excess of KI emission will occur locally on the slit. If one examines the slits located 5″ and 10″ West (panels a_1 & a_2), both show an excess emission to North compared to South. On the 5″W slit, the bump seen at North represents an emission excess of up to a factor of 5 compared to what is expected from a spherically symmetric envelope. Emission excess is also seen at West on the slits located north of the star, in consistency with indications provided by 5″ and 10″ West slits. The positions of these local maxima are roughly aligned, together with the star positions and the two holes in the molecular envelope, as emphasized by the full line in the central panel in Fig. 5. This reinforces the hypothesis of a bipolar outflow.

Previous experiments of KI scattering have suggested that potassium remains in atomic form at least in circumstellar envelopes with mass loss rates of about 10^{-7} to 3 10^{-6} M$_\odot$ yr^{-1} (see Guilain & Mauron 1996 and references therein). If one assumes that the fraction of neutral species $n_{K\,I}/n_K$ is constant in the probed regions of the envelopes, then the KI scattering intensity can be used to detect local variations of total density. More precisely, the KI intensity from a point in the envelope is proportional to the product of $n_{K\,I}(r)$ by the stellar illuminating flux $F \propto r^{-2}$, and this product has to be integrated along the line of sight (Honeycutt et al. 1980). Optical thinness is assumed in the above integration and this is actually supported by the fact that the KI doublet ratio is close to two for most of the reliable points, as shown in Fig. 6. The positions where this ratio is lower than two are mostly found on CFHT slits, and thus should correspond to observations affected by telluric absorption rather than optically thick emission (see Sect. 2.2).

A comparison between such optically thin model and the observed data from the 5″ W slit is given in Fig. 7. Apart from the emission excess clearly seen at North and discussed above, another interesting point can be noticed. The maximum emission is not centered at $\Delta\delta = 0$ but at $\sim$ +2″. A similar shift is also observed on the 10″ W slit, where emission peaks at $\Delta\delta \sim$ +4″. These shifts may reflect an asymmetry in the spherical component. We rather interpret it as an asymmetric illumination. Indeed, if one considers the density law shown in Fig. 2 with a small inclination of the northern hole towards West, stellar light may be more absorbed by the inner dust towards the South-West, where KI emission is weaker.

4. Discussion

4.1. Origin of the asymmetries of the o Ceti envelope

The *o* Ceti system (star(s) + envelope) displays asymmetries on all scales. First of all, the primary star appears elliptical on HST

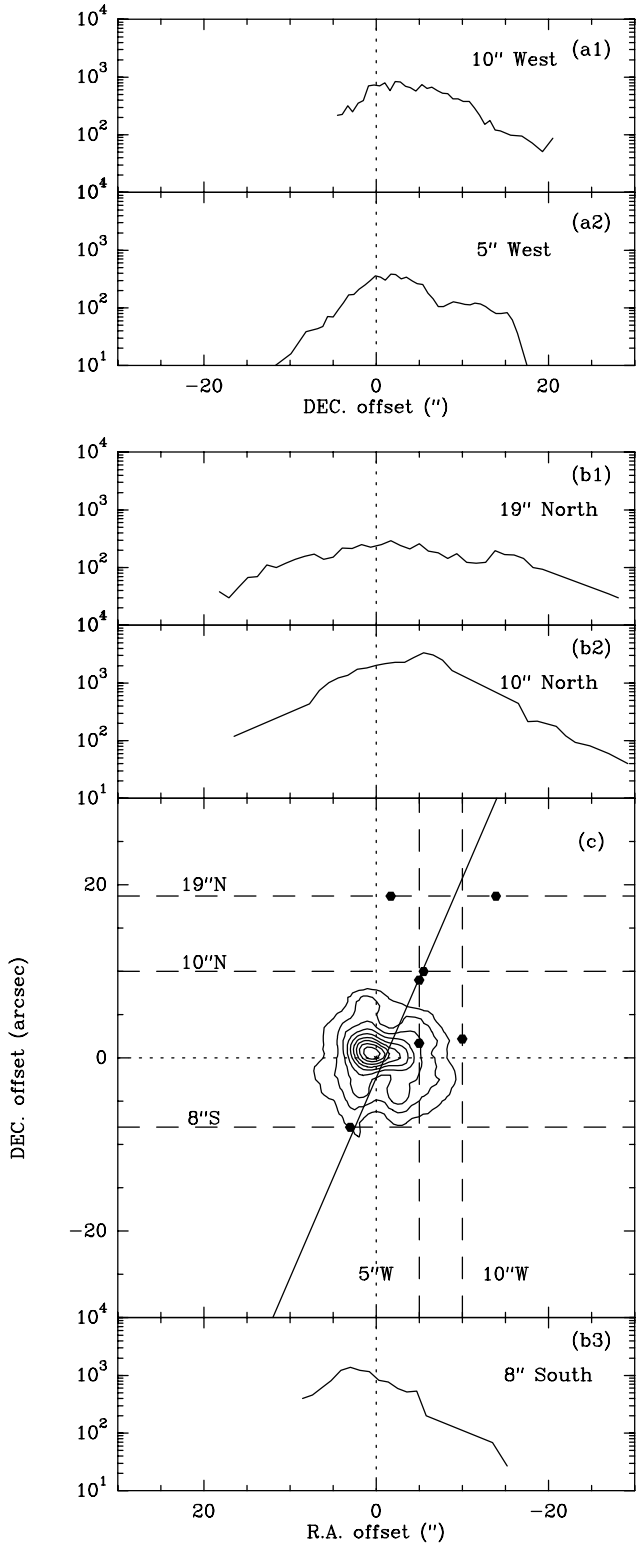

Fig. 5a–c Intensity distribution of the 7699 Å KI line along 5 slits. Panels **a1** and **a2**: the two western slits observed at CFHT. Panels **b1**, **b2** and **b3**: northern and southern slits observed at OHP. Panel **c**: location of the slits (dashed lines) superimposed on the CO(2–1) map; the black dots on each slit indicate the positions of the maxima of KI emission. The full line emphasizes the apparent alignment of some maxima with the center (see text for details).

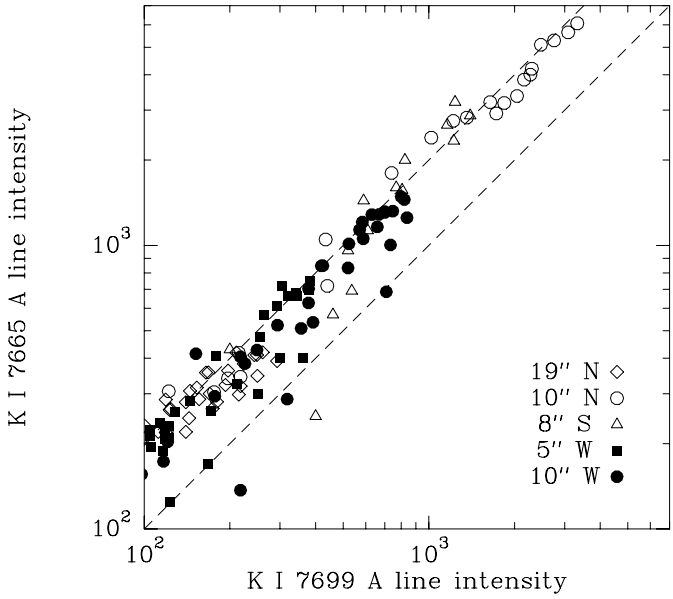

Fig. 6. Intensity of the two KI lines. The upper dashed line indicates a ratio of 2, corresponding to the optically thin case. Only the data with a good signal-to-noise ratio are plotted.

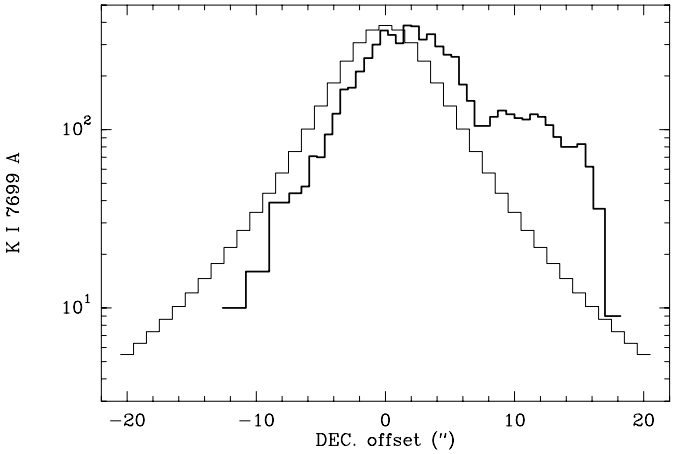

Fig. 7. Comparison between an optically thin model of KI emission in a spherical envelope (thin line) and the observations from the 5″W slit (thick line).

images (Karovska et al. 1997). The cause is unclear: it could result from bright spots on the stellar surface or in the extended atmosphere, or from non-radial pulsations. Furthermore, the UV image may reveal interaction between Mira A and Mira B, in the form of a hook in Mira A atmosphere, extending towards Mira B. This latter feature may be linked with the formation of the accretion disk, which has been detected from UV spectroscopy by Reimers & Cassatella (1985).

Infrared interferometry at 11 μm also reveals the complexity of the extended atmosphere and the inner dust envelope ($R \lesssim 10\ R_\star$; Lopez et al. 1997). These observations can be interpreted either by two or more spherical dust shells or by an inhomogeneous or clumpy envelope.

Finally, sphericity seems to appear only on the larger scales, such as in the 21 cm HI map (Bowers & Knapp 1988), the interaction of the envelope with the interstellar medium explaining the observed HI density excess. Nevertheless, the sensitivity of this map (signal-to-noise ratio $\lesssim 5$) is too low to allow the observation of any small-scale asymmetries as those observed in CO and KI. Furthermore, the low velocity of the bipolar outflow as measured in CO probably favours the smoothing of the density distribution on larger scales, explaining why it is not noticeable in the HI map.

The coupling of all these data with our observations allows to draw out some conclusions about the origin of the asymmetries. First of all, it seems clear that mass loss is not isotropic. Indeed, the two kinematic components in the CsE probably prevent from explaining the geometry by external effects such as asymmetric photodissociation of CO and photoionization of KI by UV radiation of interstellar origin or emitted by the companion star.

The observed axis of the bipolar outflow may be perpendicular to the companion orbital plane (for the orbital elements given by Reimers & Cassatella 1985), so that one could think about a link between both structures. But regarding the probable thinness of this disk (Reimers & Cassatella 1985), it is unlikely that it could collimate the outflow.

The presence of asymmetries on all scales, ranging from the star itself to the atomic envelope, suggests that they originate in the stellar atmosphere. An asymmetric mass-loss process, due to e.g. non-radial pulsations or giant convective cells and/or magnetic spots on the stellar surface, is thus the most natural explanation.

4.2. Comparison with other asymmetric envelopes around AGB stars

Our data display a patent view of strong asymmetries in the molecular and atomic circumstellar envelope of this Mira variable, which are consistent with asymmetries previously discovered on smaller scales, such as the stellar atmosphere and the inner dust envelope (e.g. Karovska 1999, 2000). Other AGB stars were already known to have such asymmetries. We discuss here the cases of X Her (Kahane & Jura 1996), V Hya (Kahane et al. 1996) and π^1 Gru (Knapp et al. 1999). All these objects were thought to represent the link between spherical envelopes around "young" mass-losing AGB stars and bipolar planetary nebulae.

X Her is oxygen-rich as o Ceti, but is a semi-regular (SR) AGB star. CO observations (Kahane & Jura 1990) put in evidence that its CsE is composed of a slowly expanding spherical envelope (V_{exp} = 2.5 km s^{-1}) and a weakly collimated bipolar outflow, with an expansion velocity $\gtrsim$ 10 km s^{-1}. X Her is not known to be a binary star, but polarization variations suggest that a companion could lie at a few stellar radii (Shawl 1975). Anyway, this companion, if present, would have a very low mass and a low UV flux, rather different from Mira B.

V Hya is a carbon-rich SR AGB star. Multi-wavelength observations (atomic and molecular gas, dust) by Kahane et al. (1996; see also references therein) show that a high velocity bipolar outflow ($V_{exp} \gtrsim$ 50 km s^{-1}) goes through a low velocity spheroidal CsE (V_{exp} = 7.5 km s^{-1}). A remarkable consideration is that the spherical expansion velocities for V Hya and o Ceti are similar, while the bipolar expansion velocity is much higher for V Hya than for o Ceti. The high rotational velocity of V Hya, close to the disruption limit, suggests that this geometry is due to the recent complete merging of a binary system and a common envelope phase.

π^1 Gru is a SR mass-losing S star, which has a companion of solar type. Knapp et al. (1999) interpreted its CO(2–1) line profile as arising from an expanding disk ($V_{exp} \simeq$ 15 km s^{-1}) and a fast bipolar outflow ($V_{exp} \gtrsim$ 70 km s^{-1}). Both expansion velocities are higher than for o Ceti, but not in the same proportion: V_{exp}(bipolar outflow)/V_{exp}(spherical envelope) $\lesssim$ 2 for o Ceti and about 5 for π^1 Gru.

All these objects thus belong to the 20% of *semiregular* AGB stars with non-isotropic mass-loss (Kahane & Jura 1996 and references therein). On the contrary, o Ceti is a regular variable. The analysis of CO(3-2) profiles of a sample of 36 O-rich Miras by Young (1995) reveals that 8 of them may have non spherical CsE, and Plez & Lambert (1994) showed that the envelope of R Leo, another Mira variable, is highly asymmetric, but o Ceti is up to now the only Mira in which a bipolar outflow is directly observed. Furthermore, regarding their mass-loss rates and IRAS colours, the three objects described above also appear more evolved.

Another remarkable fact is that the bipolar outflow always has an expansion velocity much higher than that of the spheroidal component, whereas both velocities are of the same order for o Ceti. This suggests that departure from sphericity, due to a bipolar outflow, occurs very early on the AGB, if not since the beginning. Furthermore, the bipolar outflow could accelerate as the star evolves along the AGB phase.

Finally, even if all these examples display some evidences for binarity (although quite weak for X Her), the properties of the companions, in particular their temperature and distance to the AGB star, are very different. It thus seems unlikely that binarity with such different properties could generate a similar effect, that is the formation a bipolar outflow.

We conclude that the standard view of mass loss on the AGB, based on isotropic mass loss during most of the build-up of the CsE, has to be revised. High resolution observations of young CsE are needed either to confirm this conclusion or to reveal the exceptionality of the o Ceti envelope.

5. Conclusions

We presented new high-resolution observations of the neutral envelope of o Ceti envelope. The molecular envelope, observed in the CO(2–1) radio line with a 2.5″ resolution, appears very complex and may be composed of a rather spherical envelope being disrupted by a low-velocity bipolar atomic outflow. This outflow, oriented North-South, is inclined by about 30° with respect to the plane of the sky. The extent of the molecular envelope is essentially limited by photodissociation by interstellar

UV radiation. The atomic envelope, observed in the optical KI lines, is about 4 times more extended. The bipolar outflow is also clearly visible in these lines.

o Ceti is probably a young AGB star. Our data bring new evidence that asymmetric mass loss is a common phenomenon, which occurs from the beginning of the AGB phase to the superwind and post-AGB phase. This may be particularly important to explain the shaping of bipolar Planetary Nebulae.

Acknowledgements. We acknowledge the IRAM staff from the Plateau de Bure and from Grenoble for carrying the observations and help provided during the data reduction. We are also grateful to the referee, M. Karovska, for fruitful comments. This research has made use of the Simbad database, operated at CDS, Strasbourg, France. E.J., P.P. and R.B. acknowledge partial support from spanish grants PB 96-104 and SB 97-22043, and N.M. support from the French CNRS "Physico-Chimie du Milieu Interstellaire" program.

References

Barthes D., Mattei J.A., 1997, AJ 113, 373
Bowers P.F., Knapp G.R., 1988, ApJ 332, 299
Bujarrabal V., Fuente A., Omont A., 1994, A&A 285, 247
Chaffee F.H. Jr., White R.E., 1982, ApJS 50, 169
Guilain C., Mauron N., 1996, A&A 314, 585
Guilloteau S., Delannoy J., Downes D., et al., 1992, A&A 262, 624
Haniff C.A., Ghez A.M., Gorham P.W., et al., 1992, AJ 103, 1662
Herpin F., Baudry A., Alcolea J., Cernicharo J., 1998, A&A 334, 1037
Honeycutt R.K., Bernat A.P., Kephart J.E., et al., 1980, ApJ 239, 565
Jura M., 1986, ApJ 303, 327
Kahane C., Jura M., 1996, A&A 310, 952
Kahane C., Audinos P., Barnbaum C., Morris M., 1996, A&A 314, 871
Karovska M., Nisenson P., Beletic J., 1993, ApJ 402, 311
Karovska M., Hack W., Raymond J., Guinan E., 1997, ApJ 482, L175
Karovska M., 1999, In: Le Bertre T., Lèbre A., Walekens C. (eds.) Asymptotic Giant Branch Stars. IAU Symp. 191, p. 139
Karovska M., 2000, In: Kastner J.H., Soker N., Rappaport S.A. (eds.) Asymmetrical Planetary Nebulae II, ASP Conf. Ser. Vol. 199, p. 67
Knapp G.R., Morris M., 1985, ApJ 292, 640
Knapp G.R., Young K., Lee E., Jorissen A., 1998, ApJS 117, 209
Knapp G.R., Young K., Crosas M., 1999, A&A 346, 175
Lopez B., Danchi W.C., Bester M., 1997, ApJ 488, 807
Lopez B., 1999, In: Le Bertre T., Lèbre A., Walekens C. (eds.) Asymptotic Giant Branch Stars. IAU Symp. 191, p. 409
Mamon G.A., Glassgold A.E., Huggins P.J., 1988, ApJ 328, 797
Mauron N., Caux E., 1992, A&A 265, 711
Neri R., Kahane C., Lucas R., Bujarrabal V., Loup C., 1998, A&AS 130, 1
Olofsson H., Eriksson K., Gustafsson B., Carlström U., 1993, ApJS 87, 267
Olofsson H., 1999, In: Le Bertre T., Lèbre A., Walekens C. (eds.) Asymptotic Giant Branch Stars. IAU Symp. 191, p. 3
Omont A., Lucas R., Morris M., Guilloteau S., 1993b, A&A 267, 490
Planesas P., Bachiller R., Martin-Pintado J., Bujarrabal V., 1990a, ApJ 351, 263
Planesas P., Kenney J.D.P., Bachiller R., 1990b, ApJ 364, L9
Plez B., Lambert D.L., 1994, ApJ 425, L101
Reimers D., Cassatella A., 1985, ApJ 297, 275
Reimers Ch., Dorfi E.A., Höfner S., 1999, In: Second Austrian ISO Workshop, in press
Sahai R., Wannier P.G., 1992, ApJ 394, 320
Shawl S.J., 1975, AJ 80, 602
Walmsley C.M., Chini R., Kreysa E., et al., 1991, A&A 248, 555
Wooten A., Lichten S.M., Sahai R., Wannier P.G., 1982, ApJ 257, 151
Young K., 1995, ApJ 445, 872